3D Heart Segmentation and Volumetry Using Deformable Shape Models

T Schwarz, T Heimann, I Wolf, HP Meinzer

German Cancer Research Center, Heidelberg, Germany

Abstract

Segmentation using deformable model-based approaches has become a common application in 3D medical image analysis, as it provides a fast and robust method to detect structures, e.g. organs, fully-automated after initialization. However, some earlier approaches in some cases did not converge in the segmentation process even on rather good datasets or showed major variations in the segmentation results. This work presents the application of a shape model enhanced with the possibility of free deformation with respect to local grey value distributions, used to automatically detect the end-diastolic and end-systolic left heart ventricle (LV) in 3D MRI images after a short user interaction, thus to calculate the heart stroke volume.

1. Introduction

Segmentation of medical images is a significant task to aid medical diagnostics and therapy planning. Commonly this segmentation is done manually in 2D cut planes, or with the help of semi-automated tools. As the resolution of medical images is constantly increasing, this task gets more and more time-consuming and irreproducible. Therefore, robust and fast automated methods are needed to keep up with the advances in image acquisition technology. Active shape models (ASMs), as first introduced by [1], represent such a method.

Assessment of ventricular function or volume via different imaging techniques is a common task in medical examination of the cardiac system. For quantitative analysis, segmentation is often virtually inevitable. Over the last decade, active shape models became more and more promising in the effort of fully automated segmentation. A detailed overview of different variations and approaches to ASMs for cardiac segmentation can be found in [2]. ASMs, especially combined with the possibility of free deformation, provide an excellent method for segmentations of more complex shapes. In this paper, a deformable shape model is presented, which already showed superior results in CT liver segmentation [3], and has now been adapted for MRI left ventricles. The used model shows stable convergence on all available datasets, providing excellent segmentation results.

2. Methods

2.1. Deformable shape model

The underlying model is based on a statistical shape model (SSM), gained from principal component analysis of training data, i.e. representing the mean shape and the strongest modes of variation occurring in the training data. Subsequently, local grey value gradient profile appearance models are generated for each landmark. The employed deformable model is a discrete triangular mesh of the same topology as the SSM. During the segmentation progress, internal forces drive edge lengths and angles towards the values of the best-representing SSM, i.e. the closest valid shape. At the same time, external forces pull vertices towards the optimal surface as extracted from image data. In contrast to previous approaches, not the individual best solutions for each landmark are used; instead, a graph-based algorithm for optimal surface detection that delivers a globally optimal solution is employed [4]. To increase both segmentation speed and accuracy, the model search is applied hierarchically on four resolutions of a beforehand calculated Gaussian image pyramid, from coarse to fine resolution, until the convergence criteria for the particular resolution is met.

The deformable shape model has been integrated into the Medical Imaging Interaction Toolkit (MITK) [5], and is able to segment images almost fully automated: The only necessary user interaction is the choice of a roughly estimated search starting position in the image, which in no case took more than 30 seconds per image. The same starting position could be used for both the segmentation of the diastole and the systole.

Although the initial training of an ASM is quite time-consuming, this has only to be done once, and the actual computation time of the segmentation was less then one minute per volume.

2.2. End-diastolic LV

The dataset used for evaluation of the segmentation quality consists of 22 MRI images of the upper torso, in which the left ventricle has been manually per-segmented by medical experts. The images have resolutions of 256x256x160 (19 images), 128x128x88 (1 image) and 128x128x80 (2 images), respectively. As multiple gold standard segmentations per image were available, but were varying distinctly in some cases, these where averaged for each single image using a STAPLE ground truth image filter, as described in [6].

Because not enough data was provided to separate the dataset in training and evaluation parts, leave-one-out tests were performed. Thus, 22 shape models were built, and in each case evaluated on the single volume not included in the build process.

2.3. End-systolic LV

This dataset consists of only 21 MRI images and the corresponding pre-segmentations. The images have resolutions of 256x256x160 (18 images), 128x128x88 (1 image) and 128x128x80 (2 images), respectively. All other properties are equal to the diastolic LVs. So this time, 21 models were trained and leave-one-out tests were performed.

2.4. Volumetry

The heart stroke volume (SV) is calculated as the difference between the segmented end-diastolic and end-systolic ventricle volumes, respectively. The results were compared with the differences of the given gold standard segmentations. In 13 cases, also direct measurements of the stroke volume via velocity-encoded cine MR imaging (VEC MRI, see e.g. [7]) were available and used for comparison.

3. Results

3.1. Segmentation

The segmentation results are shown in Table 1 and 2. Additionally, graphs of the average surface distance results are given in Fig. 1 and Fig. 4. An example of end-diastolic LV segmentation images is shown in Fig. 2. An example of a 3D view can be seen in Fig. 3.

As segmentation quality measures, the average symmetric point-to-surface distance and the symmetric RMS point-to-surface distance are given. These are define as follows: The distance from a point x to a surface Y is given by

$$d(x,Y) = \underbrace{\min}_{y \in Y} \|x - y\|$$

where $\|.\|$ denotes the Euclidian distance. When defining surface distances, we have to make sure to respect symmetry, a precondition for every metric. Thus, the average surface distance is defined as:

$$D_{avg}(X,Y) = \frac{1}{|X|+|Y|}\left(\int_{x \in X} d(x,Y)dx + \int_{y \in Y} d(y,X)dy\right)$$

where $|.|$ denotes the area of a surface. In a similar fashion, the root mean squared surface distance (equivalent to the RMS error) is defined as

$$D_{RMS}(X,Y) = \sqrt{\frac{1}{|X|+|Y|}\left(\int_{x \in X} d^2(x,Y)dx + \int_{y \in Y} d^2(y,X)dy\right)}$$

The last used metric is the Dice coefficient, which is a measure to quantify the similarity between two regions A and B, based on the volumetric overlap:

$$C_D = \frac{2\,|A \cap B|}{|A|+|B|}$$

where $|.|$ denotes the volume of a region. The Dice coefficient yields 1 if both shapes are identical and 0 for no overlap at all. To transform the measure into an error metric, the obvious way is to negate it. Thus, the volumetric error based on the dice coefficient is defined as:

$$V_D = 1 - C_D$$

These quality measures are compared to recent publications.

No result data was omitted due to divergence of the model search.

The clearly higher point-to-surface error of the end-systolic LVs compared to the end-diastolic is up to one main cause:

The end-diastolic volumes have a noticeable higher contrast due to the blood movement in the systolic volumes. Therefore, the diastolic ventricle boundary gradients are more significant and segmentation results are better.

Table 1. Segmentation results for the end-diastolic LVs. Results are given as mean ± standard deviation (μ±σ).

Segmentation	D_{avg}[mm]	D_{RMS}[mm]	V_{Dice}[%]
Deformable model	0.95±0.21	1.58±0.42	6.4±1.2
Lötjönen et al. [8]	2.01±0.31	n.a.	n.a.
Kaus et al. [9]	2.28±0.93	n.a.	n.a.
van Assen et al. [10]	1,97±0.54[1]	n.a.	n.a.

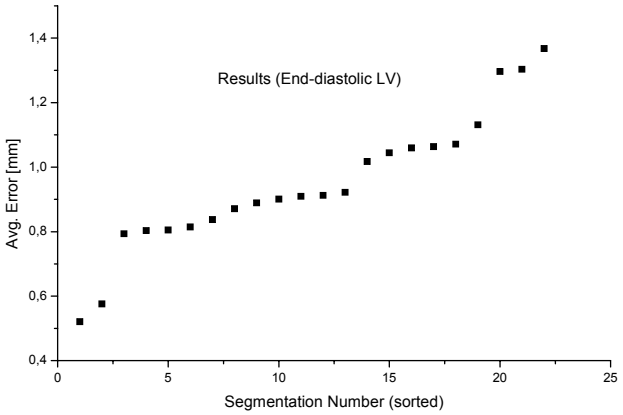

Fig. 1. Distribution of the segmentation results for the end-diastolic LV (sorted).

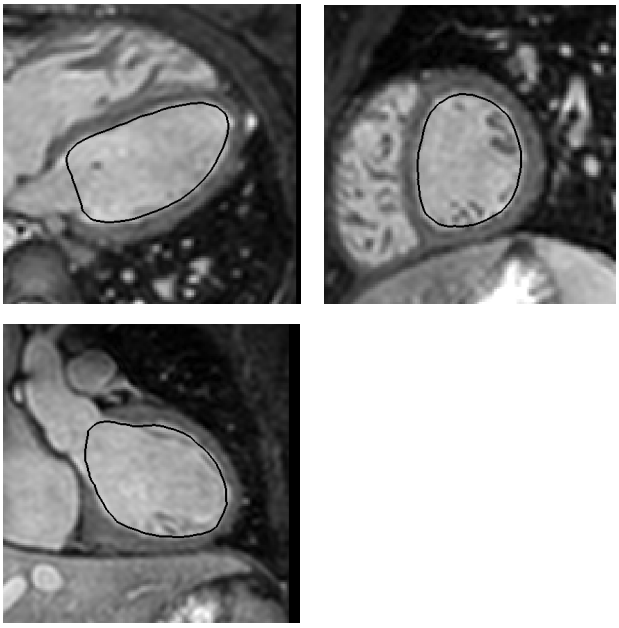

Fig. 2. Example of sagittal, transversal and coronal view of the median completed end-diastolic LV segmentation. The resulting surface is shown as a black line.

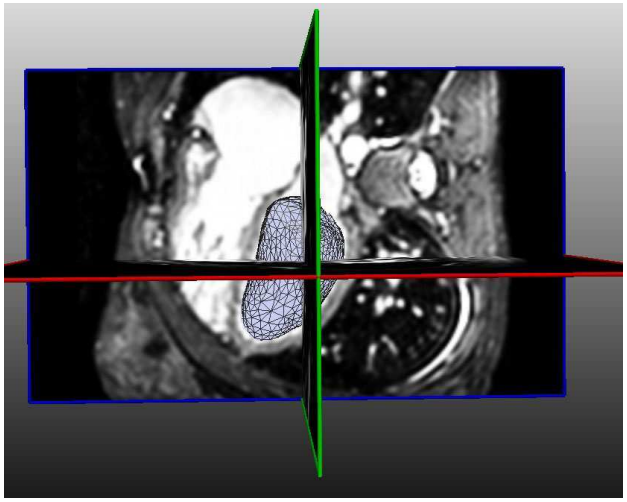

Fig. 3. 3D view of the segmentation result as a wireframe mesh. Also, the cut planes from Fig. 3 can bee seen.

Table 2. Segmentation results for the end-systolic LVs. Results are given as mean ± standard deviation (μ±σ).

Segmentation	D_{avg}[mm]	D_{RMS}[mm]	V_{Dice}[%]
Deformable model	1.69±0.68	2.48±1.01	16.2±5.3
Kaus et al. [9]	2.76±1.02	n.a.	n.a.
van Assen et al. [10]	1,97±0.54[1]	n.a.	n.a.

[1] van Assen et al. do not state the cardiac cycle stage they used their segmentation on.

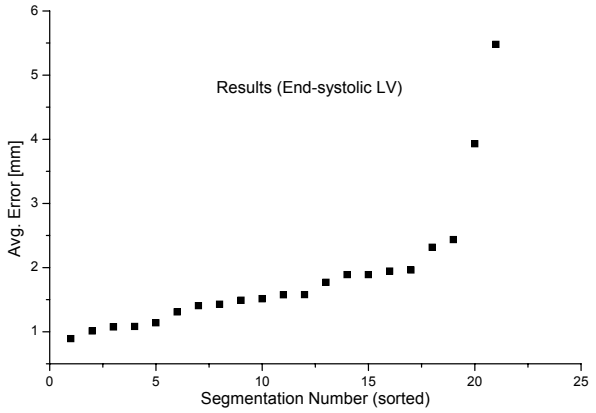

Fig. 4. Distribution of the segmentation results for the end-systolic LV (sorted).

3.2. Volumetry

In Table 3, the heart stroke volume results, compared with the direct measurement and with the calculated gold standard are given, showing the result of the computation in terms of the mean relative error (The relative error of the single results compared to the appropriate gold standard, averaged over all results). Also, the Pearson product-moment correlation coefficient is stated, giving a dimensionless measure of the linear correlation between two random variables.

Table 3. Results of the stroke volume computation, compared with two different methods of gold standard SV . In both cases, the 13 images for which the direct measurement was given are evaluated.

SV compared to:	Direct Measurement	Difference of gold standard segmentations
Mean rel. error [%]	12.4	8.4
Pearson's correlation coefficient	0.89	0.97

4. Discussion and conclusions

The deformable shape model presented in this paper shows the capability to fastly and robustly detect and segment the left heart ventricle, and is therefore applicable in a wide range of clinical applications in diagnosis and therapy aid. The free deformation terms used in this approach help to better adapt the shape model to the given data than a model strictly constricted to trained shapes.

According to experience, it is difficult to compare applications of shape models from different groups, as the presented models are almost always specialized for a certain purpose. The model introduced by [10], for example, is particularly suitable for sparse volume data.

Nevertheless, the segmentation result achieved in this work has to our best knowledge not been met by any other prior approach.

Both segmentation and volumetry results show variations from the gold standard, but approximately in the magnitude the various gold standards differ between each other.

Future plans include the evaluation of an already implemented real-time user interaction possibility to further increase segmentation quality and usability. This is especially useful if structures emerge in the volumes that were not included in the training shapes, e.g. congenital heart diseases or large tumors. Furthermore it shall be made possible to automatically segment complete (4D-) time series all of a sudden, including the calculation and visualization of the temporal deformation vector field.

References

[1] Cootes TF, Taylor JC, Cooper DH, Graham J. Active Shape Models – Their training and application. Comput Vis and Image Underst 1995; 61(1):38–59.

[2] Frangi AF, Niessen WJ, Viergever MA. Three-Dimensional Modeling for Functional Analysis of Cardiac Images: A Review. IEEE Trans Med Imag. 2001;20(1).

[3] Heimann T, Wolf I, Meinzer HP. Active Shape Models for a Fully Automated 3D Segmentation of the Liver - An Evaluation on Clinical Data. In: Proc. MICCAI 2006, LNCS 4191. Place Published: Heidelberg: Springer, 2006;41-48.

[4] Li K, Wu X, Chen DZ, Sonka M. Optimal surface segmentation in volumetric images - a graph-theoretic approach. IEEE Trans. Pattern Anal Mach Intell 2006; 28(1):119-134.

[5] Wolf I, Vetter M, Wegner I et al. The Medical Image Interaction Toolkit. Med Imag Anal 2005; 9(6):594-604.

[6] Warfield S, Zou K, Wells W. Validation of image segmentation and expert quality with an expectation-maximization algorithm. In: Proc. MICCAI 2002. Place Published: Springer, 2002;298-306.

[7] Heidenreich PA, Steffens J, Fujita N et al. Evaluation of mitral stenosis with velocity-encoded cine-magnetic resonance imaging. Am J Cardiol 1995;75(5):365-9.

[8] Lötjönen J, Kivistö S, Koikkalainen J et al. Statistical shape model of atria, ventricles and epicardium from short- and long-axis MR images. Med Image Anal 2004;8(3):371-386.

[9] Kaus MR, von Berg J, Weese J et al. Automated segmentation of the left ventricle in cardiac MRI. Med Image Anal 2004;8(3):245-254.

[10] van Assen HC, Danilouchkine MG, Frangi AF et al. SPASM: a 3D-ASM for Segmentation of Sparse and Arbitrarily Oriented Cardiac MRI Data. Med Image Anal 2006;10(2):286-303.

Address for correspondence

Tobias Schwarz
German Cancer Research Center
Im Neuenheimer Feld 280
69120 Heidelberg
tobias.schwarz@dkfz.de